Mapping brain structural differences and neuroreceptor correlates in Parkinson's disease visual hallucinations: a mega-analysis

Miriam Vignando (✉ miriam.vignando@kcl.ac.uk)
King's College London
Dominic ffytche
King's College London
Simon Lewis
University of Sydney
Phil Hyu Lee
Yonsei University
Seok Chung
Yonsei University College of Medicine
Rimona Weil
Dementia Research Centre, University College London, 8-11 Queen Square, London, WC1N 3AR
Michele Hu
Oxford University
Clare Mackay
Department of Psychiatry, University of Oxford
Ludovica Griffanti
Oxford Parkinson's Disease Centre, Oxford https://orcid.org/0000-0002-0540-9353
Delphine Pins
Univ. Lille, Inserm
Kathy Dujardin
Univ. Lille, Inserm
Jardri Renaud
Lille University https://orcid.org/0000-0003-4596-1502
John-Paul Taylor
Newcastle University
Michael Firbank
Newcastle University https://orcid.org/0000-0002-9536-0185
Grainne Mcalonan
King's College London
Henry Ka-Fung Mak

The University of Hong Kong https://orcid.org/0000-0002-2007-0650
Shu-Leong Ho
The University of Hong Kong
Mitul Mehta
King's College London https://orcid.org/0000-0003-1152-5323

Article

Keywords: Parkinson's disease, Parkinson's psychosis, MRI, structural imaging, structural covariance, neurotransmitters, visual hallucinations

Posted Date: March 9th, 2021

DOI: https://doi.org/10.21203/rs.3.rs-270425/v1

Version of Record: A version of this preprint was published at Nature Communications on January 26th, 2022. See the published version at https://doi.org/10.1038/s41467-022-28087-0.

Abstract

Parkinson's psychosis (PDP) describes a spectrum of symptoms that may arise in Parkinson's disease (PD) including visual hallucinations (VH). Imaging studies investigating the neural correlates of PDP have been inconsistent in their findings, due to differences in study design and limitations of scale. Here we use empirical Bayes harmonisation to pool together structural imaging data from multiple research groups into a large-scale mega-analysis, allowing us to apply new methodological approaches to identify cortical regions and networks involved in VH and their relation to receptor binding. Differences of cortical thickness and surface area show a wider cortical involvement underlying VH than previously recognised, including primary visual cortex and its surrounds, and the hippocampus, independent of its role in cognitive decline. Structural covariance analyses point to a strong involvement of the attentional control networks in PD-VH, while associations with receptor density maps suggest neurotransmitter loss may drive the cortical changes.

1. Introduction

Patients with Parkinson's disease (PD), aside the typical motor symptoms[1], commonly experience a variety of non-motor symptoms, including psychiatric ones[2]. Among these, visual hallucinations (VH) and related visual phenomena form a spectrum of symptoms referred to as *Parkinson's psychosis*[3] (PDP). There is a continuum of experiences with patients initially experiencing minor hallucinations (perception of presence or passage) and illusions that progress to formed hallucinations (initially with insight preserved), then hallucinations in other modalities and delusions[4]. Such symptoms may affect up to 70% of PD patients in more advanced stages of the illness[5] in the context of dopamine therapy, but do not show a clear relationship between medication introduction or dose suggesting the symptoms of PDP are not simply medication side-effects[4]. VH predict a range of poor outcomes including more rapid cognitive decline and development of dementia[6–8] and nursing home placement[9]. It is difficult to determine how VH might be related to these poor outcomes without a clear understanding of the brain systems involved in VH[4].

Imaging studies of VH in PD to date have been based on relatively small samples and have used differing designs that variously control for the degree of cognitive decline, stage of PD and dopamine medication. This makes it difficult to disentangle brain changes related specifically to VH mechanisms as distinct from those related to cognitive decline, PD stage or medication effects. As a result, a heterogeneous array of structural differences has been reported. Depending on whether or not cognition is controlled for, some studies have found volume reductions in specific regions that have not been replicated in other studies including: hippocampus[10], cerebellum[10–11], lateral, superior and medial frontal cortex[11–13], thalamus[14] and different subregions of visual association cortex, broadly defined to include the lateral occipital cortex, ventral occipito-temporal cortex (ventral stream) and visual parietal lobe (dorsal stream) [11,15,16].

A meta-analysis utilising the previously reported regional differences demonstrated very little consistency across studies, suggesting this may be due to heterogeneity in structural brain correlates of VH, varying sensitivity in multiple small studies, or the involvement at different locations of a unifying brain network whose dysfunction results in VH[17]. While meta-analytical techniques can be useful to collate findings from different studies and help understand the consistency of brain regions involved, there are limitations in their ability to include variables such as cognition, medication dose, PD stage and duration as covariates, given that these are usually incorporated into the analyses at the study level and each study contributes a different set of regions to the meta-analysis. In contrast, mega-analyses bring together subject-level data across sites in one analysis, which presents a number of advantages. These include methodological rigour, with shared quality control and pre-processing pipelines, including software version control and the ability to include unpublished data or published data that was not used in the primary analysis (e.g. structural data collected for functional imaging studies). The same experimental design model and covariates can be applied uniformly across the data set helping address design variations in previous studies. Another advantage of the increased sample size is the additional power to explore morphometric features such as cortical thickness and cortical surface area along with undertaking complex analyses, such as structural covariance. Cortical thickness and surface area are considered as orthogonal components, which are genetically unrelated[18] and can be considered separate morphometric components in ageing and disease[1,19] .The main correlate of cortical volume is cortical surface area, but volume loss is best captured by cortical thickness[19,20]. Separate measurement and analysis of these two components thus offer a better understanding of the underlying cortical changes associated with VH in PD than volume measures alone. Finally, mega-analyses create a valuable resource that can evolve and be made available to the wider neuroimaging community, especially important in PDP given that such patients are difficult to recruit and scan.

Several neurotransmitter systems have been associated with VH in PD. Initially, VHs were proposed to be a side effect of *dopaminergic* medication[21], but later evidence has led to a revision of this view. Current consensus is that dopaminergic medication interacts with disease-related susceptibility factors in PD to cause VH, rather than as a simple side effect[3]. Cholinergic pathways have also been implicated in VH[22,23], with neurodegeneration in brainstem and forebrain cholinergic nuclei[22] and electrophysiological measures of cholinergic function reduced in patients with VH[24]. Recently, a role for serotonergic dysfunction in VH has been suggested[25], linked to alterations of 5-HT2_A receptor density[26,27] (for a review[28]).

In summary, our mega-analysis of PD with VH compared to PD without VH enables analyses that are not available to smaller scale studies to help explore the mechanisms of VH. Specifically, we are able to determine the regional cortical thickness and surface area changes associated with VH and relate these morphometric features to measures of symptom severity in a subgroup where finer-grain clinical detail is available. We perform a principal component analysis to identify smaller-scale morphometric differences within a high dimensional set of regions. In addition, we perform an exploratory structural network analysis to highlight associations between regions and clusters of connections linked to VH. Structural

covariance allows us to assay covariation of differences in grey matter morphology between different brain structures, providing information on which regions similarly change in thickness or surface area. In order to understand the neurochemical associations of these changes, we also test the hypothesis that structural differences are related to the spatial variation in subtypes of receptors for which high resolution PET atlases are available (dopamine and serotonin).

2. Results

2.1 Patient characteristics

The final dataset consisted of 493 participants (193 F), of which 135 were PD-VH. Each individual study had matched their participants for age, gender, disease onset, MMSE, UPDRS-III and levodopa equivalent daily dose (LED), with few exceptions (Table 1). We also included the unpublished data in separate ANOVAs to check group similarity (Table 1), in meta-analyses (**S2**) and in an ANOVA including the whole mega-analysis sample. While the ANOVAs and the meta-analysis demonstrated we have good matching on the criteria, the mega-analysis ANOVA shows that there is a difference of 2.19 years in age [F (1,491) = 6.56, p = .01] (PD-VH = 67.85, SD = 7.74; 62 F, and PD-noVH = 65.66, SD = 8.71; 131 F) and there is a greater proportion of females in the PD-VH group (χ^2 = 3.585, p = .06).

Morphometrics were harmonised (**S1**) and we did not find significant differences in total intracranial volume (TIV) [F(1,493) = .043, p = .84] and total brain volume [F(1,493) = 2.488, p = .115], but in total gray matter volume [F(1,493) = 5.41, p = .02] (see **S2**). For the subsample of 146 patients we had additional information and a subsample analysis was performed (see **2.3**).

Table 1

Demographics and clinical information by group. Each row represents the data present in the study for each group. Not all groups could share raw clinical data. In those cases, we reported the information of the original publication to show that there was no difference within groups in terms of PD and medication. Gender was not matched for the UCL and Sidney samples, MMSE score was lower in PD-VH in the Sydney dataset, and UPDRS-III scores higher in PD-VH in the KCL dataset.

Study	N Patients	Age	Onset	MMSE	UPDRS-III	LEDD
Shin et al., 2012	46 PD-VH (23F)	71.3 ± 5.9	3.3 ± 3.0	25.3 ± 3.0	24.1 ± 10.4	482.4 ± 252.6
(Yonsey University)	64 PD-noVH	70.7 ± 5.7	2.8 ± 3.0	25.7 ± 2.9	21.6 ± 11.0	501.4 ± 167.5
	(38 F)	p = ns	p = ns	p = ns	p = ns	p = ns
Shine et al., 2012	26 PD-VH	66.6 ± 7.2	6.0 ± 3.9	28.7 ± 1.7	32.0 ± 13.4	664.3 ± 495.2
+ unpublished data	(12 F)	66.4 ± 8.6	5.4 ± 3.5	29.6 ± 1.7	27.8 ± 16.2	706.8 ± 502.7
(University of Sidney)	48 PD-noVH	p = .9	p = .5	p = .04	p = .2	p = .7
	(12 F)					
Firbank et al., 2018	11 PD-VH (2F),	75.0 ± 3	10.2 ± 8.2	25.9 ± 1.6	51.7 ± 22.2	469.9 ± 311.3
(only non-dementia data retained)	11 PD-noVH (2F)	71.7 ± 5.3	10.1 ± 7.6	27.2 ± 2.4	30.50 ± 14.73	693.4 ± 474.1
(University of Newcastle)		p = .2	p = .9	p = .2	p = .05	p = .2
Yao et al., 2014	12 PD-VH,	67.6 ± 7.4	10.0 ± 3.5	27.6 ± 2.4	20.9 ± 10.6	978.7 ± 361.3
(University of Hong Kong)	(9F)	73.4 ± 7.4	8.4 ± 5.1	28.5 ± 1.7	18.0 ± 12.9	704.9 ± 519.4
	12 PD-noVH	p = .2	p = .4	p = .09	p = .5	p = .2
	(8F)					
Lefebvre et al., 2018	18 PD-VH	62.9 ± 6.0	8.2 ± 5.3	28.0 ± 1.24	25.0 ± 8.4	859.7 ± 411.1
Unpublished structural data	(7F)	63.8 ± 2.2	7.9 ± 4.2	28.8 ± 1.20	21.8 ± 7.9	804.3 ± 297.4
(University of Lille)	16 PD-noVH	p = .2	p = .2	p = .2	p = .2	p = .7
	(4F)					

Study	N Patients	Age	Onset	MMSE	UPDRS-III	LEDD
ffytche and Lawn, 2021 **(King's College London)**	7 PD-VH (4 F) 9 PD-noVH (3 F)	66.1 ± 6.5 68.7 ± 7.2 p = .3	8.3 ± 5.2 5.8 ± 2.5 p = .2	29.7 ± 0.5 26.8 ± 4.1 p=. 06	25.6 ± 6.6 40 ± 13.4 p=. 01	759.4 ± 529.2 746.2 ± 487.1 p = .9
Oxford Discovery Cohort, unpublished * **(Baig et al., 2015; Griffanti et al. 2020)**	7 PD-VH (5F) 103 PD-noVH (36F)	63.86 ± 10.4 60.35 ± 10.4 p = .4	2.0 ± 1.0 2.4 ± 1.6 p = .5	28.7 ± 1.4 28.6 ± 1.3 p = .2	23.0 ± 12.7 23.8 ± 10.3 p = .9	978.7 ± 361.3 323.8 ± 244.3 p = .2
T1 data submitted, demographics in **Zarkali et al., 2020** **(University College London)**	19 PD-VH (13F) 86 PD-noVH (35F)	64.6 ± 8.2 64.5 ± 7.9 p = .9	4.2 ± 2.4 4.1 ± 2.5 p = .8	28.9 ± 1.6 28.9 ± 1.1 p = .9	24.1 ± 13.1 21.7 ± 11.0 p = .4	415.6 ± 162.5 461.5 ± 269.2 p = .5

** non-motor symptoms (Baig et al., 2015), T1 data (Griffanti et al., 2020) separately published, but not in a publication studying them together.*

2.2 Hallucinators (PD-VH) vs. non-hallucinators (PD-noVH) multivariate analysis of variance.

Cortical Thickness. Lower thickness in PD-VH was present in a widespread set of regions (see Fig. 1 and S3). No regions showed greater cortical thickness in PD-VH. A main effect of *age* [$F(1,492) = 3.38$, $\eta^2 = .60$, $p < .001$], *gender* [$F(1,492) = 1.51$, $\eta^2 = .40$, $p < .001$] and TIV [$F(1,492) = 2.38$, $\eta^2 = .51$, $p < .001$] was observed.

Surface area. We found reduced area in PD-VH mainly in frontal and occipital regions (see Fig. 1) (for all tables and details see **S3**). A significant main effect of *age* [$F(1,492) = 2.08$, $\eta^2 = .47$, $p < .001$], *gender* [$F(1,492) = 1.50$, $\eta^2 = .39$, $p < .001$] and *TIV* [$F(1,492) = 6.32$, $\eta^2 = .73$, $p < .001$] was observed.

Subcortical volumes. We found a lower volume for PD-VH in the bilateral amygdala (see **S3**). A significant main effect of *age* [$F(1,492) = 11.87$, $\eta^2 = .62$, $p < .001$], *gender* [$F(1,492) = 2.64$, $\eta^2 = .26$, $p < .001$] and TIV [$F(1,492) = 255.89$, $\eta^2 = .97$, $p < .001$] was observed.

2.3 Subgroup analysis.

We created a subsample for which we have Neuropsychiatric Inventory (NPI) hallucinations subscale scores (*frequency * distress*), focussing on VH. The sample consists of 146 patients (67 PD-VH, 79 PD-noVH), matched for age, gender, TIV, medication, cognition, onset and PD severity (UPDRS-III) (but see **S4** for detailed comparisons). Results from the custom multivariate ANCOVAs were overall consistent with those found for the main sample (see **S4**).

When correlating the NPI score with morphometrics, inverse correlations were significant for right hemisphere cortical thickness in the intraparietal sulcus ($r = -.24$, $p = .05$), the superior temporal sulcus ($r = -.26$, $p = .03$), the Jensen sulcus (between the anterior and posterior rami of the IPS) ($r = -.27$, $p = .03$) and the cingulum (marginalis) ($r = -.25$, $p = .05$), and a positive correlation was found with the right frontomarginal gyrus ($r = .26$, $p = .04$). Results did not change when carrying out partial correlations between NPI score and morphometrics, and with levodopa equivalent dose (LED) as covariate (see **S4**).

2.4 Receptors density maps regression models.

Receptor densities maps of D2/D3, 5-HT_{2A} and 5-HT_{1A} were parcellated using the Destrieux atlas to ensure that density and morphometric data were aligned. We explored the relationship between the differences in cortical thickness and surface area between PD-VH and PD-noVH (Fig. 2) with separate linear models for each density map. We carried out i) a model including the morphometric difference values only of regions where we found a significant difference, and ii) a model including the morphometric difference values in all regions. The maps used were independent atlases built on healthy subjects' PET data (see Methods).

Thickness. The model with 5-HT_{2A} binding potential as predictor and the mean difference as dependent variable was significant for the subset of regions where the groups differed ($\beta = -.252$, $t = -2.2$, $p = .03$), whereas no relationship was observed when considering all the atlas regions ($\beta = -.02$, $t = -.31$, $p = .75$). A similar result was observed for 5-HT_{1A} (significant regions: $\beta = -.26$, $t = -2.25$, $p = 0.03$; all regions: $\beta = .008$, $t = .092$, $p = .504$) and for D2/D3 receptors (significant regions: $\beta = -.35$, $t = -3.14$, $p = 0.002$; all regions: $\beta = .09$, $t = .95$, $p = .34$) (see Fig. 2 for methods and results). In addition, we compared the slopes of the models, finding no difference between 5-HT_{2A}, 5-HT_{1A} and D2/D3 for significant regions) (**S6**).

Surface area. The models with 5-HT_{2A} binding potential per region as predictor and the mean difference per region as dependent variable was significant, but only for regions which differed between groups ($\beta = -.22$, $t = 2.1$, $p = .038$). No relationship was observed with all regions included ($\beta = .15$, t = 1.75, p = .08). The models with 5-HT_{1A} binding potential as predictor was significant for differing regions ($\beta = .27$, slope = 0.22, $t = 2.2$, $p = .01$) and with lower significance for all regions ($\beta = .181$, $t = 2.07$, $p = .04$). When using D2/D3 as a predictor, the model was significant for significantly differing regions ($\beta = .318$, $t = 2.5$, $p = .01$) and the model for all regions showed greater significance ($\beta = .277$, $t = 3.24$, $p = .001$). In all cases, the greater the mean difference, the lower the binding potential. However, when estimating the confidence intervals of the models, the model for D2/D3 was no longer significant (**S6**). 5-HT_{2A}, 5-HT_{1A} and D2D3 slopes for significant regions did not differ (**S6**). See Fig. 2, for methods and results and **S6** for further details.

The same models were carried out also for subcortical volumes not yielding significant results for all receptors (see **S6**).

2.5 Principal components analysis (PCA).

We performed PCA to reduce the dimensionality of the dataset while preserving variability, to identify underlying clusters to clarify the results from the group-level analyses.

Cortical thickness. The PCA returned two dimensions with eigenvalues > 1 explaining 67.58% of total variance. The regions best representing Dimension 1 (eigenvalue = 4.47, 49.69% of variance) as assessed with the cosine squared index were the left superior frontal gyrus, the left middle frontal gyrus and the bilateral precentral gyrus. The regions best representing Dimension 2 (eigenvalue = 1.61, 17.89% of variance) were the cuneus, and the occipital superior gyrus, bilaterally (see Fig. 3a; for scree plots see **S7**).

Surface area. The PCA returned two components with eigenvalues > 1. Dimension 1 (eigenvalue = 4.48, 56.01% of variance) and Dimension 2 (eigenvalue = 1.38, 17.21% % of variance) for a total cumulative variance of 73.23% of explained variance. For Dimension 1, the contributing regions were visual regions: left and right calcarine sulci, the right occipitotemporal lingual gyrus and the right occipital pole. For Dimension 2, the contributing regions were the left central insular area, the anterior and superior portions of the circular sulcus of the insula (Fig. 3.**b**, **S7**).

For cortical thickness only, we found a significant inverse correlation of Dimension 1 individual contributions and NPI score (r = .-138, p = .049). In addition, the thickness for the Dimension 1 regions (left SFG, MFG, precentral) negatively correlated with NPI score (r =-.15, p = .046, one-tailed Pearson correlation), with the individuals having higher pathological score having also the lower thickness in these regions.

2.6 Structural covariance analysis.

To explore and characterise the gray matter morphology covariation and network-level organisation of PD-VH and PD-noVH patients for cortical thickness and surface area we performed structural covariance analyses.

After specifying a general linear model for each region, the structural covariance matrices (68x68) for each group was defined by estimating the inter-regional correlation between model residuals of thickness and area (in separate models).

Cortical thickness. Significant difference of the two covariance matrices (PD-VH, PD-noVH) was first tested (χ^2 = 3010.82, df = 2278, z of differences = 3.83). The cell-by-cell comparisons of residuals' inter-regional correlation coefficients highlighted differences in interregional covariance, in particular in the left inferior temporal gyrus, supramarginal gyrus and inferior parietal lobe (IPL), superior frontal (SFG) and inferior frontal gyrus (IFG) pars opercularis and the fusiform and lateral occipital gyri on the right (Fig. 4). Overall, inter-regional correlations were greater for the PD-VH group (but see also **S8**).

Hubs, that is nodes (here regions) that are thought to strongly contribute to the global network function, were identified in frontal, parietal and occipital regions for the PD-noVH group, and in frontal, temporal and parietal regions for the PD-VH group (Fig. 5a). Permutation tests for vertex-level measures returned differences in betweenness centrality, which was greater in PD-VH in the left and right lingual gyrus, in the left lateral occipital gyrus and the right SPL ($p\ FDR < .05$). Communities are sets of brain regions characterised by denser and stronger relations among themselves, if compared with regions of other communities. Structural covariance-based communities have been found to replicate neighbourhoods observed with seed-based approaches in fMRI and DTI (see Methods for details). The first community in the PD-VH group comprised mainly occipitotemporal regions, with the second involving parietal and some frontal regions. In the PD-noVH group, the first community consisted of mostly frontoparietal regions whereas the second comprised occipitoparietal regions (Fig. 5b). In addition, the PD-noVH group showed higher modularity, as assessed with bootstrapping (*mean* = 0.29 *SD* = 0.02, *CI* 0.25, 0.36 at density 13%) (for communities by lobe, see **S8**).

Surface area. As for thickness, the two covariance matrices were different (χ^2 = 5347.2, *df* = 2278, *z* of differences = 6.8). In addition, among the others, significant differences in interregional covariance were observed bilaterally in the rostral MFG, STS, fusiform gyrus, and IPL; in the left caudal MFG, lateral occipital gyrus, SPL, and insula and in the right anterior and posterior cingulate, and IFG pars opercularis, with a pattern very similar to the one observed for thickness (see Fig. 6 and S8).

Hubs were identified mainly in occipitotemporal and frontal regions for the PD-noVH group and in frontal, temporal and occipital regions for the PD-VH group (Fig. 7). In accordance with this result, vertex-level permutation tests returned differences in betweenness centrality the left fusiform gyrus; in addition, differences were observed for the middle orbitofrontal gyrus, IFG orbitalis and triangularis, and in the bilateral anterior cingulate ($p < .003$, $p_{FDR} < .09$), whereby centrality was greater for PD-noVH in these regions, but greater for PD-VH in the left caudal MFG and in the right SFG. The first community in the PD-VH group is characterised by occipitotemporal and frontal and the second community by occipito-parietal and parietal regions only (Fig. 7b; representation by lobe is in S8). In addition, PD-noVH showed greater modularity, as assessed with bootstrapping (0.29, CI 0.21, 0.36 density 13%).

Finally, we found a significant positive correlation between difference of the surface area means in the NPI subsample and with the difference in local efficiency ($r = .24$, $p = 0.02$), whereby the greater the difference in the surface area, the greater the difference in the local efficiency. The regions with both the greatest area differences and efficiency differences were the bilateral lingual gyrus, lateral occipital gyrus, right cuneus and right insula.

3. Discussion

We have presented a mega-analysis of patients with Parkinson's disease with and without visual hallucinations, demonstrating widespread alterations in brain structure, with differential effects for cortical thickness and surface area and examined their relationship to receptor distributions and network-

level effects. Below we discuss the implications of the findings and their relationship to current theories of VH.

Cortical thickness and surface area

Cortical thickness and surface area (SA) are considered two separate components in ageing and disease[1,19] reflecting different aspects of the neurodegenerative process. Cortical thickness loss relates to cortical layering and, by inference, cytoarchitecture, while surface area relates to gyral anatomy and, by inference, underlying white matter. Widespread reductions in *cortical thickness* in hallucinators were identified in the occipital, parietal, temporal, frontal and limbic lobes. The regions of reduced thickness encompassed all cortical regions identified in previous structural imaging studies (for a review[29]), suggesting previous variability may relate to stochastic effects introduced by relatively smaller samples and design differences. With the larger sample of the mega-analysis, the extent of cortical regions involved appears wider than previously suspected. However, not all regions are equally affected and, notably, there appears to be a posterior asymmetry with relative sparing of the left ventral visual stream (ventral occipito-temporal cortex) compared to the homologous region in the right hemisphere. This region plays a key role in all models of VH in PD but a greater involvement of the right hemisphere has not been noted previously. The PCA analysis helped define key sub-regions within the extensive areas of cortical thinning that contributed most to the group difference, identifying a frontal and an occipital dimension. Of these, the cuneus bilaterally and left dorso-medial aspect of the superior frontal gyrus emerged as the dominant components. These regions have been reported in previous studies but do not play a prominent role in accounts of VH in PD. The cuneus is one of the earliest regions to show cortical atrophy in PDP[30], while cortical thinning in the dorso-medial superior frontal gyrus has been reported in patients, months to years prior to the development of VH[4]. It may be that the prominence of these regions in the mega-analysis relates to the longer duration of these changes compared to other brain regions resulting in a greater consistency of thickness reduction between patients.

For *SA*, the differences between groups were more circumscribed with bilateral medial occipital SA reduction for patients with VH in a region corresponding to the primary visual cortex and its surrounds (striate and extra-striate cortex) and the left insula. This is the first-time such extensive structural changes have been identified in the primary visual cortex and its surrounds in PD patients with VH and helps account for wide-ranging low-level visual deficits found (for a review[32]). These regions also have reduced cortical thickness but their prominence in the SA analysis may imply additional gyral atrophy, sulcal widening and a reduction of underlying white matter.

The mega-analysis also allowed us to move beyond a binary comparison of VH versus noVH to examine brain regions linked to VH severity (NPI hallucination subscale) and taking into account any variability associated with age, gender, TIV, medication, cognition, disease onset and PD severity. Regions with reduced thickness for higher severity scores were found in posterior parietal, posterior cingulate and superior temporal cortex. Previous studies have associated these regions with mental rotation and visuospatial transformation[33] and imagery[34] for the IPS, and biological motion detection[35] for the STS.

These processes are altered in patients with PD and VH[36,37], thus one can infer an involvement of these processes and these regions in VH severity. In addition, the IPS is also part of the dorsal attentional network, previously implicated in VH in PD[38] (see discussion below). These regions were also identified as hubs in the structural covariance analysis, discussed further below. We cannot disentangle whether these correlations are driven primarily by the frequency or distress of VH as these measures were only available for part of the subsample. However, this is the first time a link between cortical structural changes and phenomenological aspects of VH severity has been identified.

Subcortical regions, hippocampus and cerebellum

In addition to the detailed analysis of the cerebral cortex we were able to examine the volumes of subcortical structures as well. Bilateral volume reduction was found in the amygdalae. Lewy bodies have been found in the basolateral nucleus of the amygdala associated with VH in PD patients at a similar level of cognitive impairment to those studied here[39] that may account for this finding. Unlike the amygdala, there are only sparse Lewy bodies in the hippocampus at this disease stage and volume changes in this structure are more difficult to interpret. Since the prevalence of VH increases as PD progresses, it is difficult to disentangle brain changes related primarily to cognitive decline from those related primarily to VH or that may contribute equally to both. Reductions of hippocampal volume have been found in some, but not all, studies of VH in PD, depending on whether patients are matched for cognitive decline[10,40]. Here we found smaller left (and a trend for right) hippocampus in the NPI sample where we were able to covary for age, gender, TIV, onset, LED, PD severity and cognition. The volume reductions in the NPI analysis cannot be explained by differences in cognition or PD progression between groups, confirming a role for the hippocampus in the mechanism of VH that is independent of cognition[10], thus highlighting the need to carefully design studies and control for cognitive and disease factors when examining hippocampal contributions to VH. The thalamus has been suggested as a key hub linking several cortical networks associated with VH in PD[17]. We did not find altered thalamic volumes, suggesting that any functional changes in this structure are not associated with volume loss. Finally, reduced volume in cerebellar lobules VIII, IX/VII and Crus 1 is associated with VH in PD[41]. Freesurfer does not segment specific cerebellar subfields but volume changes were found in cerebellar white matter that may relate to these cerebellar cortical changes[41].

Neurotransmitter receptor density and structural imaging changes

There is only sparse Lewy body pathology in the cortex of PD patients with VH at the disease stage included in our analysis[39], raising the question of what causes the extensive cortical changes found in this and previous studies. One possibility is that such cortical changes represent synaptic loss secondary to degeneration in neurotransmitter inputs to the cortex. Previous studies have found changes in cholinergic, serotonergic, dopaminergic and GABAergic systems in PD patients with VH[25,26,36]; however, the relationship between regions of cortex with volume loss and the cortical distribution of these neurotransmitter systems has yet to be examined. We were able to investigate this relationship for

subtypes of dopamine and serotonin receptors for which high resolution maps are available and found that cortical regions with higher binding had increased cortical volume loss. The association, in particular for 5-HT_{2A}, was confined to regions linked to VH rather than the cortex as a whole, suggesting the neurotransmitter effects were specific to VH, consistent with the possibility that degeneration in these neurotransmitter systems in PD underlies synaptic loss and cortical thinning. 5-HT_{2A} and 5-HT_{1A} binding maps were correlated so the same cortical regions are likely to have contributed to both serotonin findings. While increased binding was associated with increased thickness loss, the opposite association was found for SA, with higher binding exhibiting less SA reduction. This finding was not specific to VH regions for dopamine and 5-HT_{1A} so may reflect a different process to the thickness alterations found. It is also unclear what causes low binding regions to be associated with increased loss of SA.

Structural covariance

The examination of inter-regional correlations, with areas sharing reductions in thickness or SA considered part of a functionally connected network, showed that regions of greater inter-regional thickness correlation in PD-VH overlap with those of the dorsal and ventral attention networks (DAN and VAN)[42], with the notable addition of para-hippocampal regions. Most of these regions of higher covariance have reduced thickness in PD-VH, suggesting the covariance is driven by correlated reductions in thickness. Dysregulation of VAN, DAN and default mode networks (DMN) have been implicated in models of VH in PD[38] with reduced activity in the DAN of PD-VH[43], and the inter-regional covariance findings support this view. In contrast, the inter-regional SA covariance findings highlight key DMN regions in medial frontal and posterior cingulate cortex. These regions were not found to have reduced SA in PD-VH, suggesting a relative preservation of the DMN compared to VAN and DAN. Indeed, results from dynamic fMRI have indicated active coupling between the DMN and the visual network, which correlated with the frequency of misperceptions, as opposed to reduced connectivity between the DMN, VAN and DAN[44]. Hub metrics for thickness in the occipital lobe and parietal lobe were stronger in patients with VH, suggesting cortical thinning has a wider impact on the network in these patients, highlighting the importance of functional alterations in early visual areas in VH. One could argue that VH may not only depend upon on areas presenting neural pathology, but also on areas that may be relatively unaffected but operate in a network where there is pathology elsewhere, thus becoming functionally pathological while structurally intact[45]. Indeed, all the regions where richness of connections was either lower or higher for PD-VH fell outside areas of reduced SA in VH, suggestive of a more functional pathology which needs to be further explored with functional connectivity. Finally, of particular note was the extent, in the hub analysis, of interconnected areas in the ventral, lateral and medial temporal lobe that was larger in the PD-VH group. These regions had reduced thickness in PD-VH implying the local extent of thickness reduction is greater in PD-VH.

Strengths and limitations

This is the first mega-analysis of VH in PD, pooling data to create the largest sample of PD patients with and without VH tested to date. While this is a major strength of the study, it also introduces complexities

that smaller studies do not have to address. One is the variability of clinical data available for each site, limiting the analyses we could perform with the full dataset of 493 participants. This means that some of the key analyses, for example those related to clinical covariates, could only be carried out in a smaller sample of 146 participants, but this is still substantially larger than any previous study. Another complexity is the need to address variance in the data caused by scanning at different sites and scanner types. Previous studies have typically used voxel-based methods to examine structural differences between PD-VH and PD-noVH. We used a different method to allow us to harmonise data between sites and examine cortical thickness and SA separately, but this means our findings are not directly comparable to those of previous studies. The primary focus of the study is on the cerebral cortex so we have not attempted to examine the detailed anatomy of regions such as the basal ganglia, hippocampus, cerebellum and thalamus that may have a role in VH. Finally, we do not have access to high resolution density maps for cholinergic receptor subtypes which limits the range of neurotransmitter analyses we can perform.

Conclusions

The mega-analysis has allowed us to resolve several uncertainties in the previous literature and describe new features of the VH phenotype in PD. With a sufficiently large sample, more widely distributed cortical involvement emerges than previously suspected with the important novel finding of involvement of the primary visual cortex and its surrounds. Structural covariance modelling has helped dissect out networks linked to attentional control within the widespread cortical regions affected, adding further evidence for the role of these networks in PD-VH. The findings also help resolve ambiguities between structural correlates of general cognitive decline or PD progression and those specifically related to VH. Patients at the same stage of PD and general cognitive impairment who experience VH have lower hippocampal volumes than those who do not. The hippocampus does not currently play a central role in models of VH in PD and our findings suggest this needs to be reconsidered. We can argue that the hippocampus represents part of an extended DMN composed of functional hubs, a dorsal medial subsystem and a medial temporal subsystem, which includes the hippocampus[46]. Thus, structural covariance, graph-level analyses and structural hippocampal imaging point to the involvement of attentional control networks in PD-VH. Finally, the findings shed light on why widespread cortical changes occur at a stage of PD with only sparse cortical neuropathology. The associations between dopaminergic and serotonergic receptor binding and cortical thickness provide the first evidence that the cortical changes may be driven by neurotransmitter reductions, raising the possibility of novel interventions to mitigate these effects at an earlier stage of disease.

4. Methods

4.1 Studies selection

Based on the literature, we identified N=17 studies of VH in patients with PD that included acquisition of T1-weighted structural MRI scan, as part of a structural or functional data analyses, and with patients

meeting our inclusion criteria (see below). We contacted the research groups responsible for the studies and among those N=8 groups took part in the project, offering previously published and/or unpublished data: Prof. Simon Lewis[44] (University of Sydney), Prof. Phil Hyu Lee and Dr. Chung[47] (Yonsei University), Prof. Henry Mak, Prof. Grainne McAlonan and Prof. S.L. Ho[40] (King's College London and The University of Hong Kong,), Prof. Kathy Dujardin, Prof. Renaud Jardri and Dr. Delphine Pins[48](University of Lille), Prof. John-Paul Taylor and Dr. Michael Firbank[36] (Newcastle University), Dr. Rimona Weil[49] (University College London,), Prof. Michele Hu, Prof. Clare Mackay and Dr. Ludovica Griffanti[50,51] (Oxford Parkinson's Centre Discovery Cohort), Dr. Dominic ffytche[41] (King's College London) (see **Table 1** in the Results section for details). Only data from participants diagnosed as dementia-free were included to minimise the contribution to the study of global cortical changes in patients with PD dementia. The study (LRS-19/20-17680) was given ethical approval by King's College London Research Ethics Office, Psychiatry, Nursing and Midwifery (PNM) Research Ethics Panel on the 25/03/2020 and was subsequently pre-registered on the Open Science Framework site on 04/05/2020 (https://osf.io/nzatk). The methods follow the pre-registered plan with the addition of exploratory graph theoretical analyses based on structural covariance (section 4.3.4 and results in section 2.6).

4.2 Participants

Raw T1-weighted MRI scans were obtained from 8 different groups for a total of 519 subjects. We used 493 MRI scans in the analysis after discarding N=20 participants who did not meet the criteria in terms of diagnosis (e.g. healthy controls, with diagnosis of dementia) or whose scan did not segment well during pre-processing and subsequent troubleshooting steps or was not suitable for analysis (e.g. motion) (N=6). Patients with a MMSE score below 24 (raw) were retained (N=8) only when part of a published work in which the absence of dementia was specifically stated. The final sample comprised 493 participants, 135 with VH, 358 without VH (further details in *Results* section and in **Table 1** and **S2**). Hallucination data collection varied across groups, as several used a different scale to screen for VH. Each group had previously divided patients into PD-VH and PD-noVH and we retained these original groupings for the mega-analysis.

4.3 MRI data pre-processing and harmonisation

MRI data was pre-processed with Freesurfer 6.0.0[52] to estimate cortical thickness, surface area and subcortical volumes. Data was processed on King's College London HPC infrastructure Rosalind (https://rosalind.kcl.ac.uk), with the standard recon-all procedure, consisting of motion correction, skull-stripping, affine registration to Talairach atlas, segmentation, smoothing, and parcellation mapping. In order to screen for possible errors in the segmentation process, mean cortical thickness measures and manual slice by slice inspection were used to identify possible errors in the white-grey matter boundary and pial reconstruction steps. For subjects that did not segment properly the failed processing steps were re-run (autorecon3) after performing the appropriate corrections. Low quality scans (e.g. with excessive motion, n= 4) or scans that did not segment well upon troubleshooting (n =2) were discarded. Individual cortical thickness, subcortical volumes and surface area measures were extracted based on the Destrieux

atlas[53]. In order to explore structural differences between patients with and without VH across the different cohorts minimising variance due to different recruitment sites and, therefore, different scanners, we used a harmonisation method. ComBat is an empirical Bayesian algorithm aiming at minimising the variance due to the scanner features and to maintain the variance related to biological features and has been previously successfully used in studies of cortical thickness[54-55]. In this study, this method has been also used to harmonise volume and surface area for each participant (see **Supplemental information S1** for more details about this method and plotted results).

4.3.1 Group differences analysis

First, we conducted a meta-analysis with R package 'metafor'[56] to check whether patients were matched on the relevant demographic and clinical variables. Results are mentioned in the main text and reported with forest plots and a detailed description in **Supplemental Information S2**.

Then, we conducted separate exploratory ANOVAs and MANCOVAs for cortical thickness, surface area and subcortical volumes to screen for group differences between hallucinators and non-hallucinators, with age, gender and total intracranial volume (TIV) as covariates (when appropriate upon checking assumptions; see *Results* and Supplemental Information **S2**). Multiple comparisons were Bonferroni corrected. The models were calculated using SPSS 24.0.0.0 (IBM corp. 2016) and R 4.0.0 (R core team, 2017). Results are presented in **Figure 1**, created with a custom colour coding based on *p* values and by overlaying region labels on a brain render.

We used Tukey's method programmed in R with the 1.5*IQR rule to identify outliers other than those excluded upon unsuccessful pre-processing. This allowed the careful inspection of the identified subjects in order to verify whether the outlier value depended upon measure errors (e.g. harmonisation bugs) or incorrectly entered data, or on the subject, with the purpose of retaining outliers depending on the subject (e.g. intrinsic features of the subject). No participants were discarded upon this check for this analysis.

4.3.2 Sensitivity and Subgroup analysis.

Of the eight original groups, three used the Neuropsychiatric Inventory (NPI) to score visual hallucinations. For this subgroup of studies, patients were matched for age, gender, onset, levodopa equivalent daily dose (LEDD), and Mini Mental State Examination (MMSE) score. Within each of the 3 studies, patients were also matched in terms of motor symptoms severity (UPDRS-III). We also ran a one-way ANOVA to check whether the subsample was matched for UPDRS-III but data was missing for 20 participants. We computed the group mean and used that to fill the missing value for the between groups multivariate ANOVA. We carried out Pearson's product moment correlation coefficient between NPI score and the cortical thickness, surface area and subcortical volume data; we computed the same analysis with LED as a covariate in order to address its potential role in VH severity. In addition, we compared the PD-VH and PD-noVH in the data set using the original VH binary scores to check for consistency in the results with the larger data set, including age, gender, disease onset, LED, PD severity (UPDRS-III) and MMSE as covariates (**Supplemental Information S4**). We also conducted analyses of variance with a

larger subgroup and with graded VH scores (mild, moderate, severe), together with an ordinal logistic regression (for details on the sample, methods and results see **Supplemental Information S5**).

4.3.3 Receptor density profiles.

Regression models with the difference of the means (VH – noVH) of morphometrical features (thickness, surface area, subcortical volume) as dependent variable and receptors density profiles as predictors were carried out, a methodology previously used on brain volumes[57]. Specifically, receptors density profiles were obtained for D2/D3, 5-$HT1_A$ and 5-$HT2_A$ based on a [^{18}F] Fallypride template[58] and a [11C] Cumi-101 5-HT_{1A} and a [11C] Cimbi-36 5-HT_{2A} templates[59], respectively. We have focussed on DA and 5-HT as high resolution templates are available for these receptors of interest at the moment. Including cholinergic maps in the analysis would greatly enrich this approach given the importance of cholinergic transmission in VH in PD (as described in the introduction) and will be done once high resolutions templates will be available. [^{18}F] Fallypride is a D2/D3 receptor antagonist with a high signal to noise ratio[60]. [11C] Cumi-101 and [11C] Cimbi-36 are high affinity PET radioligands for 5-$HT1_A$ and 5-$HT2_A$ receptors[59] (Beliveau et al., 2017). Parametric modelling of the binding potential used the cerebellum as reference region[61] and thus the vertices corresponding to the cerebellum were excluded from the regression analyses. Each of these templates was registered to the Talairach space using the *fsaverage* template subject and parcellated with the Destrieux atlas, to ensure alignment with the parcellated structural data of our participants. For each of the vertices we extracted the binding potential using *fslmeants*. Regression models were carried out to estimate the relationship between cortical thickness and surface area differences of the mean between VH and noVH patients (regions resulting from the first group-level MANCOVAs and ANOVAs, see **2.1**, **S3**) and receptor density profiles. For surface area, we used regions that resulted different in PD-VH vs. PD-noVH from an exploratory one-way ANOVA, as the number of regions resulting different in the basis of the MANCOVAs performed and reported in S3 were too small in number to carry out a more powered model. We ran separate models for each receptor and for thickness, surface area and volume. In addition, for each receptor we ran three different models. First, we examined the relationship between the receptor's binding potential in the regions with significant differences in cortical thickness/surface area between PD-VH and PD-noVH. The sloopes for these models were also compared (**Supplemental Information S6**). Then, in order to better investigate such relationship, we also assessed whether the receptor's binding potential could predict thickness/area values for all regions; finally, with the same purpose, we ran models considering only regions where the difference between the groups was not significant (**S6**). Linear regression models were coded in R using the packages rstatix[62] (Kassambara, 2020) and MASS[63]. For each regression model, in order to identify outliers, Cook's distance was computed and any data point with a Cook's distance >1 was marked as highly influential, explored and if appropriate discarded[64]. In addition, the confidence intervals of the significant regression models were estimated with the bootstrapping technique[65] with 100,000 cycles (**S6**). Methods and results for thickness and surface area are graphically represented in Figure 3, for results on volume and further details see **Supplemental Information S6**).

4.3.4 Principal component analysis (PCA).

Results from the MANCOVAs comparing PD-VH and PD-noVH highlighted the involvement of widespread cortical regions in a high dimensional dataset. We used principal component analysis (PCA), in order to reduce the dimensionality of the dataset and to identify putative latent dimensions underlying the differences in structure in PD-VH versus PD-noVH patients while retaining as much variance as possible[66]. Data from both hemispheres was entered in each model (one for cortical thickness, one for surface area). Analyses were carried out with R packages *factominer*[67] and *factoextra*[68]. The scree plots for the PCA are reported in **S7**. Separate PCAs were carried out for thickness and surface area. PCA inputs comprised the significantly different regions from the MANCOVAs (**S3**). Results are presented in Figure 3, created with a custom colour coding based on the components and by overlaying region labels on a brain render. To further explore a possible relationship of PCA components and hallucination severity, we carried out correlational analyses (Pearson product-moment) between the individual contributions to the different PCA dimensions, the NPI scores in the NPI subsample and the mean thickness and surface area of each dimension/component, that is the mean thickness/area across the regions constituting that component.

4.3.5 Structural covariance and graph theory analysis

In order to investigate inter-regional properties to explore and characterise the gray matter network-level organisation of PD-VH, we built networks based on structural covariance, a technique that assays covariation of differences in grey matter morphology between different brain structures across a specific population[69]. Since the most widely used atlas for this kind of analysis is the Desikan-Killiany atlas[70] (see also[71]), we extracted morphometric features (thickness, surface area) at the 68 vertices of this atlas. The dataset was harmonised for multi-site effects with the same procedure described in section *4.3.1*. The dataset was reduced to 467 cases as the design matrix based on the full dataset was not invertible due to high collinearity of some columns. We discarded N=26 subjects comingfrom the smallest datasets and the problem was overridden. Homogeneity of groups was verified with a Levene's test[72,73] .

The dataset counts 467 subjects, 118 PD-VH, 349 PD-noVH, with participants being matched for age. *Age* and *gender* were used as covariates in the models. Analyses were carried out with R package *braingraph*[74] and *igraph*[75]. To construct the networks, first we specified a general linear model for each region (thickness/area as outcome variable, age and gender as covariates). The structural covariance matrices of the two groups were defined by estimating the inter-regional correlation between model residuals of thickness and area (in separate models) (e.g.[76]) to build a 68x68 matrix. A density-based threshold[77] was applied to the matrix in order to retain a percentage of the most positive correlations as non-zero elements in a binary adjacency matrix. Different densities ranging from 0.05 to 0.20 with a 0.01 step size were explored. The differences between PD-VH and PD-noVH covariance matrices were then computed, first to establish that the two matrices differed significantly from one another; secondly, a cell by cell comparison was carried out to establish which covariance patterns were significantly greater for the PD-VH group compared to the PD-noVH group. Random undirected and unweighted graphs were

created for each group, and vertex- and graph-level metrics were computed for each group. For visualisation purposes a density of 0.13 was selected. Vertex importance was assessed using degree, betweenness centrality and nodal efficiency. A hub was categorised as such if its betweenness centrality was greater than the mean plus 1 standard deviation - calculated on all vertices at the same density[78-82]. To assess network segregation in order to better understand the communities observed, we used modularity, which is a measure of the strength of network partitions. High modularity is a measure of how much vertices from the same community are more connected to each other. Modularity was computed with the Louvain algorithms, which also partitioned the network in communities[83]. Cortical thickness-based networks have been shown to have distinct modules/communities of regions, similar to those derived from fMRI and DTI data[78]. Network analyses were performed with permutation tests (5000 cycles) and bootstrapping analyses to compare vertex-level measures. Results were false discovery rate corrected.

Finally, to further assess the relationship between graph level metrics and visual hallucinations in the full sample, we computed Pearson's correlation coefficients between the difference of the means of graph metrics of interest (vulnerability, transitivity, local and nodal efficiency, path length, betweenness centrality, eccentricity, distance) for the models on thickness and surface area separately, and the difference of the means in thickness and in surface area, respectively, with the NPI subsample, for which we have all clinical and demographic information and in which participants are matched on all those variables.

Declarations

Data and code availability*:* The datasets generated during this study will be made available upon publication at the project page on the Open Science Framework https://osf.io/fv2k7/registrations.

Declaration of Interests

Dr. Rimona Weil has received speaker honoraria from GE Healthcare.

Prof. Hu reports funding/grant support from Parkinson's UK, Oxford NIHR BRC, University of Oxford, CPT, Lab10X, NIHR, Michael J Fox Foundation, H2020 European Union, GE Healthcare and the PSP Association. She also received payment for Advisory Board attendance/consultancy for Biogen, Roche, CuraSen Therapeutics, Evidera, Manus Neurodynamica and the MJFF Digital Health Assessment Board, outside the submitted work.

J-P.T. has received speaker honoraria from GE Healthcare and acted as consultant for Kwoya-Kirin and received funding from Sosei-Heptares. These have no association with the present publication. J-P.T reports funding/grant support from Newcastle NHIR BRC based at Newcastle upon Tyne Hospitals NHS Foundation Trust and Newcastle University.

References

1. Dickerson, B. C., Feczko, E., Augustinack, J. C., Pacheco, J., Morris, J. C., Fischl, B., & Buckner, R. L. (2009). Differential effects of aging and Alzheimer's disease on medial temporal lobe cortical thickness and surface area. *Neurobiology of aging*, *30*(3), 432–440.
2. Schapira, A. H., Chaudhuri, K. R., & Jenner, P. (2017). Non-motor features of Parkinson disease. *Nature Reviews Neuroscience*, *18*(7), 435.
3. Ravina, B., Marder, K., Fernandez, H. H., Friedman, J. H., McDonald, W., Murphy, D., … Goetz, C. (2007). Diagnostic criteria for psychosis in Parkinson's disease: report of an NINDS, NIMH work group. *Movement Disorders*, *22*(8), 1061–1068.
4. ffytche, D.H., Creese, B., Politis, M., Chauhuri, K.R., Weintraub, D., Ballard, C. and Aarsland, D. (2017). The psychosis spectrum in Parkinson disease. *Nature Reviews*, 13(2), pp.81–95.
5. Levin et a Levin, J., Hasan, A., & Höglinger, G. U. (2016). Psychosis in Parkinson's disease: identification, prevention and treatment. *Journal of Neural Transmission*, *123*(1), 45–50
6. Aarsland, D., Andersen, K., Larsen, J. P., & Lolk, A. (2003). Prevalence and characteristics of dementia in Parkinson disease: an 8-year prospective study. *Archives of neurology*, *60*(3), 387–392.
7. Anang, J. B., Gagnon, J. F., Bertrand, J. A., Romenets, S. R., Latreille, V., Panisset, M., … Postuma, R. B. (2014). Predictors of dementia in Parkinson disease: a prospective cohort study. *Neurology*, *83*(14), 1253–1260.
8. Uc, E. Y., McDermott, M. P., Marder, K. S., Anderson, S. W., Litvan, I., Como, P. G., … Growdon, J. C. (2009). Incidence of and risk factors for cognitive impairment in an early Parkinson disease clinical trial cohort. *Neurology*, *73*(18), 1469–1477.
9. Goetz, C. G., & Stebbins, G. T. (1993). Risk factors for nursing home placement in advanced Parkinson's disease. *Neurology*, *43*(11), 2222–2222.
10. Ibarretxe-Bilbao, N., Ramirez-Ruiz, B., Tolosa, E., Marti, M. J., Valldeoriola, F., Bargallo, N., & Junque, C. (2008). Hippocampal head atrophy predominance in Parkinson's disease with hallucinations and with dementia. *Journal of neurology*, *255*(9), 1324–1331.
11. Watanabe, H., Senda, J., Kato, S., Ito, M., Atsuta, N., Hara, K., … Sobue, G. (2013). Cortical and subcortical brain atrophy in Parkinson's disease with visual hallucination. *Movement Disorders*, *28*(12), 1732–1736.
12. Sanchez-Castaneda, C., Rene, R., Ramirez-Ruiz, B., Campdelacreu, J., Gascon, J., Falcon, C., … Junque, C. (2010). Frontal and associative visual areas related to visual hallucinations in dementia with Lewy bodies and Parkinson's disease with dementia. *Movement Disorders*, *25*(5), 615–622.
13. Gama, R. L., Bruin, V. M. S., Távora, D. G. F., Duran, F. L., Bittencourt, L., & Tufik, S. (2014). Structural brain abnormalities in patients with Parkinson's disease with visual hallucinations: a comparative voxel-based analysis. *Brain and cognition*, *87*, 97–103.
14. Shin, S., Lee, J. E., Hong, J. Y., Sunwoo, M. K., Sohn, Y. H., & Lee, P. H. (2012). Neuroanatomical substrates of visual hallucinations in patients with non-demented Parkinson's disease. *Journal of*

Neurology, Neurosurgery & Psychiatry, *83*(12), 1155–1161.

15. Goldman, J. G., Stebbins, G. T., Dinh, V., Bernard, B., Merkitch, D., deToledo-Morrell, L., & Goetz, C. G. (2014). Visuoperceptive region atrophy independent of cognitive status in patients with Parkinson's disease with hallucinations. *Brain*, *137*(3), 849–859.
16. Ramirez-Ruiz, B., Martí, M. J., Tolosa, E., Gimenez, M., Bargallo, N., Valldeoriola, F., & Junque, C. (2007). Cerebral atrophy in Parkinson's disease patients with visual hallucinations. *European journal of neurology*, *14*(7), 750–756.
17. Weil, R. S., Hsu, J. K., Darby, R. R., Soussand, L., & Fox, M. D. (2019). Neuroimaging in Parkinson's disease dementia: connecting the dots. *Brain communications*, *1*(1), fcz006.
18. Panizzon, M. S., Fennema-Notestine, C., Eyler, L. T., Jernigan, T. L., Prom-Wormley, E., Neale, M., … Xian, H. (2009). Distinct genetic influences on cortical surface area and cortical thickness. *Cerebral cortex*, *19*(11), 2728–2735.
19. Storsve, A. B., Fjell, A. M., Tamnes, C. K., Westlye, L. T., Overbye, K., Aasland, H. W., & Walhovd, K. B. (2014). Differential longitudinal changes in cortical thickness, surface area and volume across the adult life span: regions of accelerating and decelerating change. *Journal of Neuroscience*, *34*(25), 8488–8498.
20. Im, K., Lee, J. M., Lyttelton, O., Kim, S. H., Evans, A. C., & Kim, S. I. (2008). Brain size and cortical structure in the adult human brain. *Cerebral cortex*, *18*(9), 2181–2191.
21. Goodwin, F. K. (1971). Psychiatric side effects of levodopa in man. *Jama*, *218*(13), 1915–1920.
22. Janzen, J., Van't Ent, D., Lemstra, A. W., Berendse, H. W., Barkhof, F., & Foncke, E. M. J. (2012). The pedunculopontine nucleus is related to visual hallucinations in Parkinson's disease: preliminary results of a voxel-based morphometry study. *Journal of neurology*, *259*(1), 147–154.
23. Collerton, D., Perry, E., & McKeith, I. (2005). Why people see things that are not there: a novel perception and attention deficit model for recurrent complex visual hallucinations. *Behavioral and Brain Sciences*, *28*(6), 737–757.
24. Manganelli, F., Vitale, C., Santangelo, G., Pisciotta, C., Iodice, R., Cozzolino, A., … Santoro, L. (2009). Functional involvement of central cholinergic circuits and visual hallucinations in Parkinson's disease. *Brain*, *132*(9), 2350–2355.
25. Ballanger, B., Strafella, A. P., van Eimeren, T., Zurowski, M., Rusjan, P. M., Houle, S., & Fox, S. H. (2010). Serotonin 2A receptors and visual hallucinations in Parkinson disease. *Archives of neurology*, *67*(4), 416–421.
26. Yasue, I., Matsunaga, S., Kishi, T., Fujita, K., & Iwata, N. (2016). Serotonin 2A receptor inverse agonist as a treatment for Parkinson's disease psychosis: a systematic review and meta-analysis of serotonin 2A receptor negative modulators. *Journal of Alzheimer's Disease*, *50*(3), 733–740.
27. Huot, P., Johnston, T. H., Darr, T., Hazrati, L. N., Visanji, N. P., Pires, D., … Fox, S. H. (2010). Increased 5-HT2A receptors in the temporal cortex of parkinsonian patients with visual hallucinations. *Movement disorders*, *25*(10), 1399–1408

28. Powell A, Ireland C, Lewis SJG. Visual Hallucinations and the Role of Medications in Parkinson's Disease: Triggers, Pathophysiology, and Management. (2020) J Neuropsychiatry Clin Neurosci. Fall;32(4):334–343. doi: 10.1176/appi.neuropsych.19110316. Epub 2020 May 6. PMID: 32374649.
29. Lenka, A., Jhunjhunwala, K. R., Saini, J., & Pal, P. K. (2015). Structural and functional neuroimaging in patients with Parkinson's disease and visual hallucinations: a critical review. *Parkinsonism & related disorders*, *21*(7), 683–691.
30. Pagonabarraga, J., Soriano-Mas, C., Llebaria, G., López-Solà, M., Pujol, J., & Kulisevsky, J. (2014). Neural correlates of minor hallucinations in non-demented patients with Parkinson's disease. *Parkinsonism & related disorders*, *20*(3), 290–296.
31. ffytche, D.H., Pereira, J.B., Ballard, C., Chaudhuri, K.R., Weintraub, D. & Aarsland, D. (2017), 'Risk factors for early psychosis in PD: insights from the Parkinson's Progression Markers Initiative', *Journal of neurology, neurosurgery, and psychiatry*, vol. 88, no. 4, pp. 325–331. https://doi.org/10.1136/jnnp-2016-314832
32. Rimona S. Weil, Anette E. Schrag, Jason D. Warren, Sebastian J. Crutch, Andrew J. Lees, Huw R. Morris, Visual dysfunction in Parkinson's disease (2016) *Brain*, Volume 139, Issue 11, Pages 2827–2843, https://doi.org/10.1093/brain/aww175
33. Papadopoulos, A., Sforazzini, F., Egan, G., & Jamadar, S. (2018). Functional subdivisions within the human intraparietal sulcus are involved in visuospatial transformation in a non-context-dependent manner. *Human brain mapping*, *39*(1), 354–368.
34. Tian, X., Zarate, J. M., & Poeppel, D. (2016). Mental imagery of speech implicates two mechanisms of perceptual reactivation. *Cortex*, *77*, 1–12.
35. Sokolov, A. A., Zeidman, P., Erb, M., Ryvlin, P., Friston, K. J., & Pavlova, M. A. (2018). Structural and effective brain connectivity underlying biological motion detection. *Proceedings of the National Academy of Sciences*, *115*(51), E12034-E12042.
36. Firbank, M. J., Parikh, J., Murphy, N., Killen, A., Allan, C. L., Collerton, D., … Taylor, J. P. (2018). Reduced occipital GABA in Parkinson disease with visual hallucinations. *Neurology*, *91*(7), e675-e685.
37. Shine, J. M., Keogh, R., O'Callaghan, C., Muller, A. J., Lewis, S. J., & Pearson, J. (2015). Imagine that: elevated sensory strength of mental imagery in individuals with Parkinson's disease and visual hallucinations. *Proceedings of the Royal Society B: Biological Sciences*, *282*(1798), 20142047.
38. Shine JM, O'Callaghan C, Halliday GM, Lewis SJ. (2014a) Tricks of the mind: Visual hallucinations as disorders of attention. Prog Neurobiol. 2014 May;116:58–65. doi:10.1016/j.pneurobio.2014.01.004. Epub 2014 Feb 10. PMID: 24525149.
39. Harding, A. J., Stimson, E., Henderson, J. M. & Halliday, G. M. Clinical correlates of selective pathology in the amygdala of patients with Parkinson's disease. *Brain* 125, 2431–2445
40. Yao, N., Shek-Kwan Chang, R., Cheung, C., Pang, S., Lau, K. K., Suckling, J., … Ho,S. L. (2014). The default mode network is disrupted in Parkinson's disease with visual hallucinations. *Human brain mapping*, *35*(11), 5658–5666.
41. Lawn and ffytche 2020 Cortex (in press)

42. Corbetta, M., & Shulman, G. L. (2002). Control of goal-directed and stimulus-driven attention in the brain. *Nature reviews neuroscience*, *3*(3), 201–215.
43. Shine, J. M., Halliday, G. M., Gilat, M., Matar, E., Bolitho, S. J., Carlos, M., …Lewis, S. J. (2014b). The role of dysfunctional attentional control networks in visual misperceptions in Parkinson's disease. *Human Brain Mapping*, *35*(5), 2206–2219.
44. Shine JM, Muller AJ, O'Callaghan C, Hornberger M, Halliday GM, Lewis SJ. (2015) Abnormal connectivity between the default mode and the visual system underlies the manifestation of visual hallucinations in Parkinson's disease: a task-based fMRI study. NPJ Parkinsons Dis. 1:15003. doi: 10.1038/npjparkd.2015.3. PMID: 28725679; PMCID: PMC5516559.
45. Ffytche, D. H. (2008). The hodology of hallucinations. *Cortex*, *44*(8), 1067–1083.
46. Qi, H., Liu, H., Hu, H., He, H., & Zhao, X. (2018). Primary disruption of the memory-related subsystems of the default mode network in Alzheimer’s disease: resting-state functional connectivity MRI study. *Frontiers in aging neuroscience*, *10*, 344.
47. Shin, S., Lee, J. E., Hong, J. Y., Sunwoo, M. K., Sohn, Y. H., & Lee, P. H. (2012). Neuroanatomical substrates of visual hallucinations in patients with non-demented Parkinson's disease. *Journal of Neurology, Neurosurgery & Psychiatry*, *83*(12), 1155–1161.
48. Lefebvre, S., Baille, G., Jardri, R., Plomhause, L., Szaffarczyk, S., Defebvre, L.,… Dujardin, K. (2016). Hallucinations and conscious access to visual inputs in Parkinson’s disease. *Scientific reports*, *6*(1), 1–10.
49. Zarkali, A., McColgan, P., Leyland, L. A., Lees, A. J., Rees, G., & Weil, R. S. (2020). Fiber-specific white matter reductions in Parkinson hallucinations and visual dysfunction. *Neurology*, *94*(14), e1525-e1538.
50. Baig, F., Lawton, M., Rolinski, M., Ruffmann, C., Nithi, K., Evetts, S. G., … Hu,M. T. (2015). Delineating nonmotor symptoms in early Parkinson's disease and first-degree relatives. *Movement Disorders*, *30*(13), 1759–1766.
51. Griffanti, L., Klein, J. C., Szewczyk-Krolikowski, K., Menke, R. A., Rolinski, M.,Barber, T. R., … Rumbold, J. (2020). Cohort profile: the Oxford Parkinson’s Disease Centre Discovery Cohort MRI substudy (OPDC-MRI). *BMJ open*, *10*(8), e034110.
52. Fischl, B. (2012). FreeSurfer. *Neuroimage*, *62*(2), 774–781.
53. Destrieux CE, Halgren E, Dale AM, Fischl B, Sereno MI (1998) Variability of the human brain studied on the flattened cortical surface. Soc Neurosci Abstr 24:1164.
54. Fortin, J. P., Cullen, N., Sheline, Y. I., Taylor, W. D., Aselcioglu, I., Cook, P.A., … McInnis, M. (2018). Harmonization of cortical thickness measurements across scanners and sites. *Neuroimage*, *167*, 104–120.
55. Radua, J., Vieta, E., Shinohara, R., Kochunov, P., Quidé, Y., Green, M., … Nenadic,I. (2020). Increased power by harmonizing structural MRI site differences with the ComBat batch adjustment method in ENIGMA. *NeuroImage*, 116956.

56. Viechtbauer W (2010). “Conducting meta-analyses in R with the metafor package.” *Journal of Statistical Software*, **36**(3), 1–48. https://www.jstatsoft.org/v36/i03/.
57. Selvaggi, P., Hawkins, P. C., Dipasquale, O., Rizzo, G., Bertolino, A., Dukart, J.,… Zelaya, F. (2019). Increased cerebral blood flow after single dose of antipsychotics in healthy volunteers depends on dopamine D2 receptor density profiles. *NeuroImage*, *188*, 774–784.
58. Dunn, J. T., Clark-Papasavas, C., Marsden, P., Baker, S., Cleij, M., Kapur, S., …Reeves, S. J. (2013). Establishing test–retest reliability of an adapted [18F] fallypride imaging protocol in older people. *Journal of Cerebral Blood Flow & Metabolism*, *33*(7), 1098–1103.
59. Beliveau, V., Ganz, M., Feng, L., Ozenne, B., Højgaard, L., Fisher, P. M., … Knudsen,G. M. (2017). A high-resolution in vivo atlas of the human brain's serotonin system.*Journal of Neuroscience*, *37*(1), 120–128.
60. Mukherjee, J., Christian, B. T., Dunigan, K. A., Shi, B., Narayanan, T. K., Satter, M., & Mantil, J. (2002). Brain imaging of 18F-fallypride in normal volunteers: Blood analysis, distribution, test-retest studies, and preliminary assessment of sensitivity to aging effects on dopamine D-2/D-3 receptors. *Synapse*, *46*(3), 170–188.
61. Ichise, M., Liow, J. S., Lu, J. Q., Takano, A., Model, K., Toyama, H., … Carson, R.E. (2003). Linearized reference tissue parametric imaging methods: application to[11C] DASB positron emission tomography studies of the serotonin transporter in human brain. *Journal of Cerebral Blood Flow & Metabolism*, *23*(9), 1096–1112.
62. Kassambara, A. (2020). rstatix: Pipe-Friendly Framework for Basic Statistical Tests. R package version 0.5.0. https://CRAN.R-project.org/package=rstati
63. Ripley, B., Venables, B., Bates, D. M., Hornik, K., Gebhardt, A., Firth, D., & Ripley, M. B. (2013). Package ‘mass’. *Cran r*, *538*, 113–120.
64. Cook, R. D., & Weisberg, S. (1982). Criticism and influence analysis in regression. *Sociological methodology*, *13*, 313–361.
65. Efron, B., & Tibshirani, R. (1986). Bootstrap methods for standard errors, confidence intervals, and other measures of statistical accuracy. *Statistical science*, 54–75.
66. Jolliffe, I. T., & Cadima, J. (2016). Principal component analysis: a review and recent developments. *Philosophical Transactions of the Royal Society A: Mathematical, Physical and Engineering Sciences*, *374*(2065), 20150202.
67. Lê, S., Josse, J. & Husson, F. (2008). FactoMineR: An R Package for Multivariate Analysis. *Journal of Statistical Software*. 25(1). pp. 1–18.
68. Kassambara, A., & Mundt, F. (2017). Package ‘factoextra’. *Extract and visualize the results of multivariate data analyses*, *76*.
69. Lerch, J. P., van der Kouwe, A. J., Raznahan, A., Paus, T., Johansen-Berg, H., Miller,K. L., … Sotiropoulos, S. N. (2017). Studying neuroanatomy using MRI. *Nature Neuroscience*, *20*(3), 314–326.
70. Desikan, R. S., Ségonne, F., Fischl, B., Quinn, B. T., Dickerson, B. C., Blacker,D., … Albert, M. S. (2006). An automated labeling system for subdividing the human cerebral cortex on MRI scans into gyral

based regions of interest. *Neuroimage*, *31*(3), 968–980.

71. Carmon, J., Heege, J., Necus, J. H., Owen, T. W., Pipa, G., Kaiser, M., … Wang, Y.(2020). Reliability and comparability of human brain structural covariance networks.*NeuroImage*, *220*, 117104.
72. Nimon, K. F. (2012). Statistical assumptions of substantive analyses across the general linear model: a mini-review. *Frontiers in psychology*, *3*, 322.
73. Cheung, M. (2019). Four covariance structure models for canonical correlation analysis: A COSAN modeling approach.
74. Watson, C. G. (2019). brainGraph: Graph Theory Analysis of Brain MRI Data. R package version 2.7.2. https://github.com/cwatson/brainGraph
75. Gabor Csardi and Tamas Nepusz. The igraph software package for complex network research. (2016) InterJournal, Complex Systems, 1695(5):1
76. He Y, Chen ZJ, Evans AC (2007) Small-world anatomical networks in the human brain revealed by cortical thickness from MRI. Cereb Cortex 17: 2407–2419. Medline
77. Fornito, A., Zalesky, A., & Bullmore, E. (2016). *Fundamentals of brain network analysis*. Academic Press.
78. Watson, C. G., Stopp, C., Newburger,J.W., and Rivkin, M. J.,. (2018) Graph theory analysis of cortical thickness networks in adolescents with d-transposition of the great arteries. *Brain and Behavior*, 8(2). ISSN 2162–3279. doi:10.1002/brb3.834.
79. Bernhardt, B. C., Chen, Z., He, Y., Evans, A. C., & Bernasconi, N. (2011). Graph-theoretical analysis reveals disrupted small-world organization of cortical thickness correlation networks in temporal lobe epilepsy. Cerebral Cortex, 21(9), 2147–2157.
80. Hosseini, S. H., & Kesler, S. R. (2013). Influence of choice of null network on small-world parameters of structural correlation networks. PLoS One, 8(6), e673
81. Tijms, B. M., Möller, C., Vrenken, H., Wink, A. M., de Haan, W., van der Flier, W. M., & Barkhof, F. (2013). Single-subject grey matter graphs in Alzheimer's disease. PLoS One, 8(3), e58921.
82. Wang, D., Shi, L., Liu, S., Hui, S. C., Wang, Y., Cheng, J. C., & Chu, W. C. (2013). Altered topological organization of cortical network in adolescent girls with idiopathic scoliosis. PLoS One, 8(12), e83767
83. Blondel, V. D., Guillaume, J.-L., Lambiotte, R., & Lefebvre, E. (2008). Fast unfolding of communities in large networks. Journal of Statistical Mechanics: Theory and Experiment,2008(10), P10008

Figures

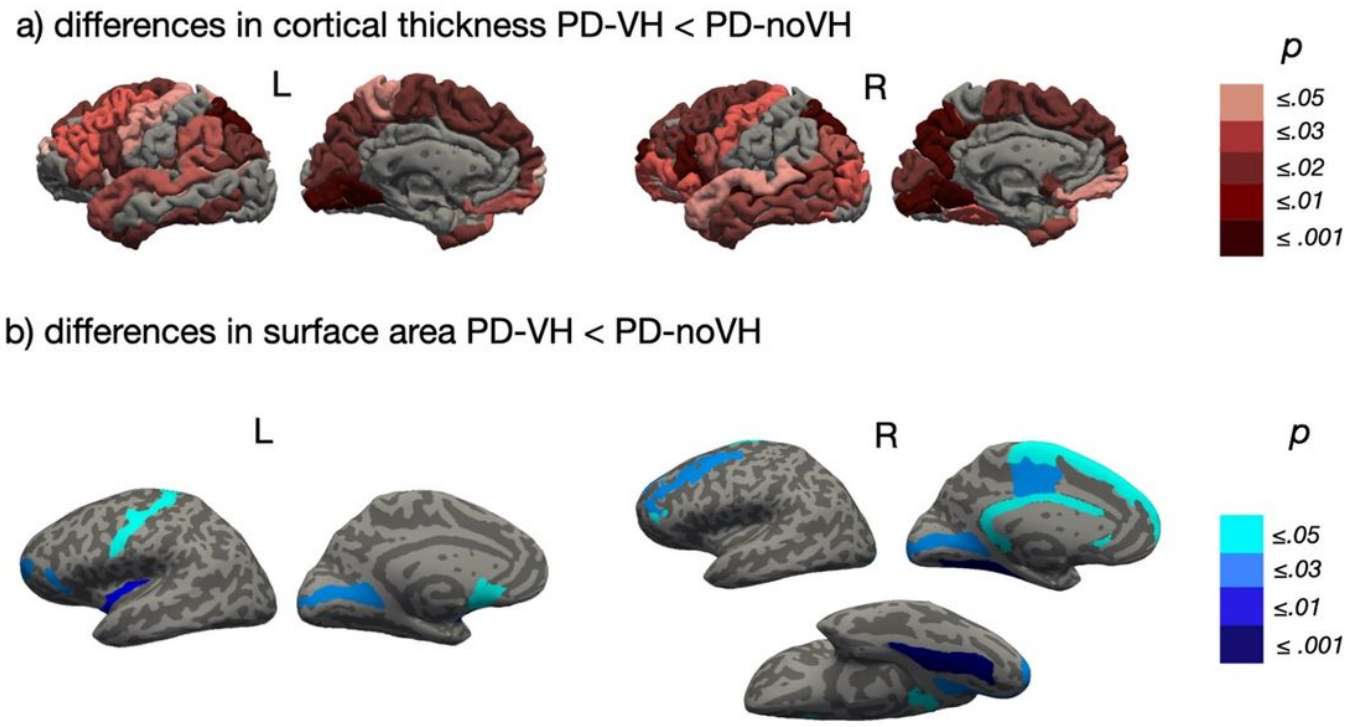

Figure 1

Group differences for PD-VH vs. PD-noVH. Shown are regions whereby PD-noVH had decreased (a) cortical thickness and (b) surface area (SA). Regions are colour coded by p value (S3). (a) Widespread decreased thickness was found in PD-VH; the regions with the greatest effect size were medial occipital parietal and frontal regions. (b) SA was reduced in PD-VH in the left and right medial occipital and in the left insular gyrus, and in the medial central and superior frontal regions. Results are corrected for multiple comparisons.

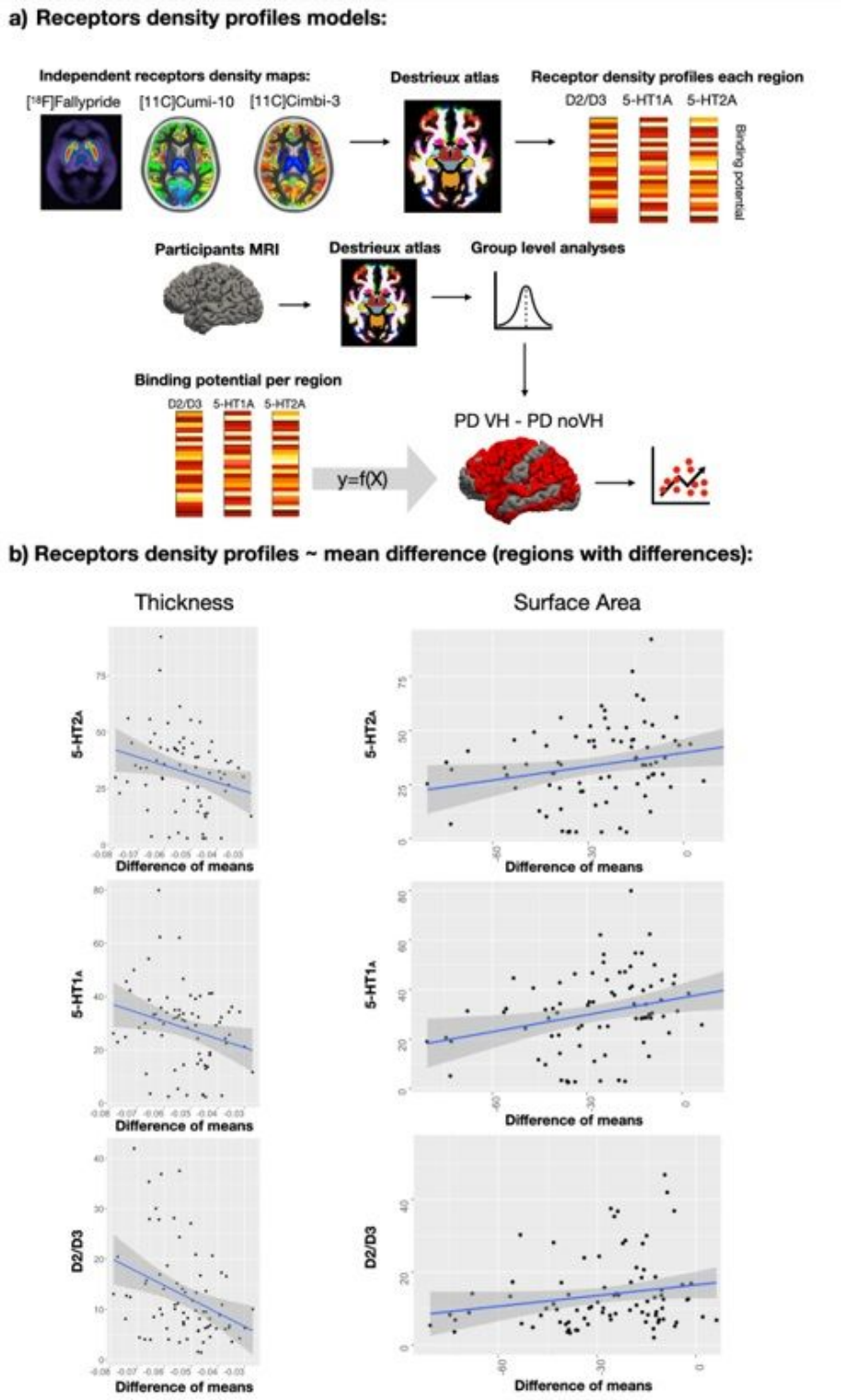

Figure 2

Receptors density profiles: methods and main results. a) Procedure and rationale of the regression models. Both the independent receptor density maps and our participants' MRI scans were parcellated with the Destrieux atlas. Cortical thickness and SA values were extracted for each region of the atlas for the participants' scans, and binding potential was extracted for each region of the atlas for the receptor density maps. Each receptor's binding potential was used in separate models as a predictor of difference

of the means of thickness/SA between PD-VH and PD-noVH. b) Results of regression models. Shown are the results of the models with the regions which were different between groups as dependent variable. Results are reported for 5-HT2A, 5-HT1A and D2/D3 receptors binding potential and thickness on the left and binding potential and SA on the right.

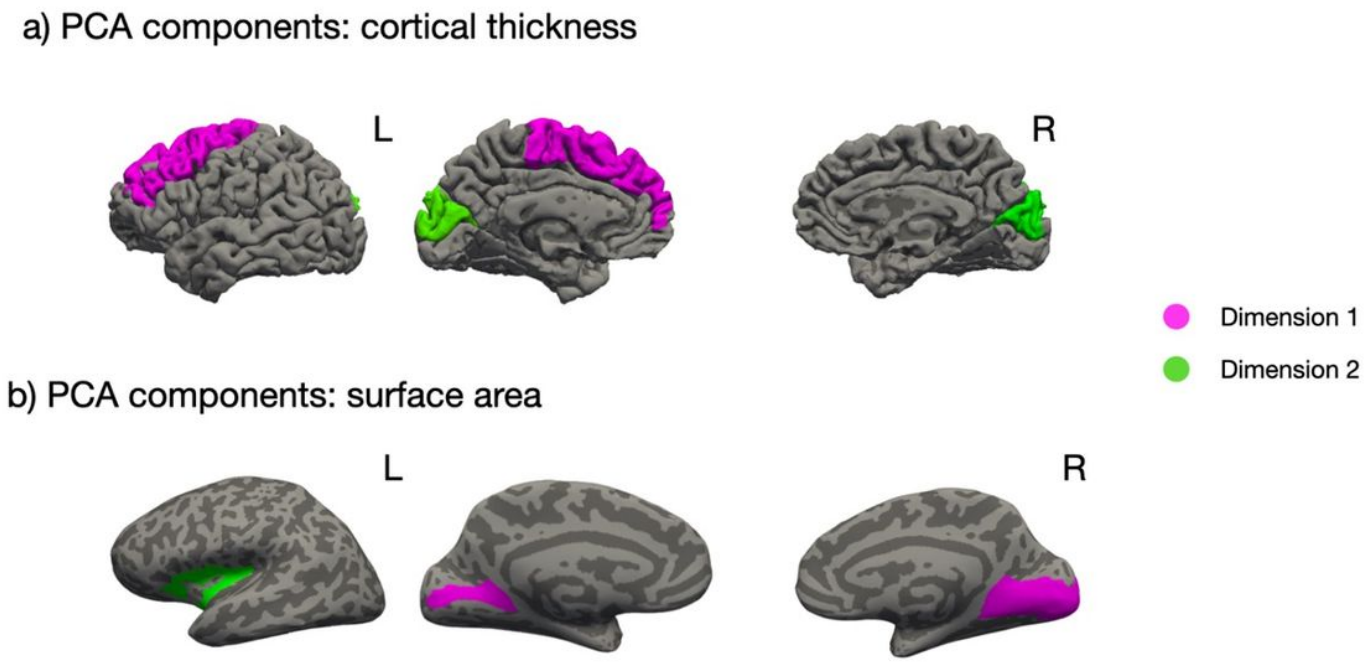

Figure 3

Graphical representation of the regions contribution to each of the Dimensions resulting from the PCA. a) Regions contributing to dimension1 and 2, cortical thickness. Dimension 1 (pink): left superior frontal gyrus, the left middle frontal gyrus and the bilateral precentral gyrus. Dimension 2 (green): bilateral cuneus and occipital superior gyrus. B) Regions contributing to dimension 1 and 2 for surface area. Dimension 1 (pink): left and right calcarine sulci, right occipitotemporal lingual gyrus, right occipital pole, Dimension 2 (green) left central insular area, anterior and superior portions of the circular sulcus of the insula.

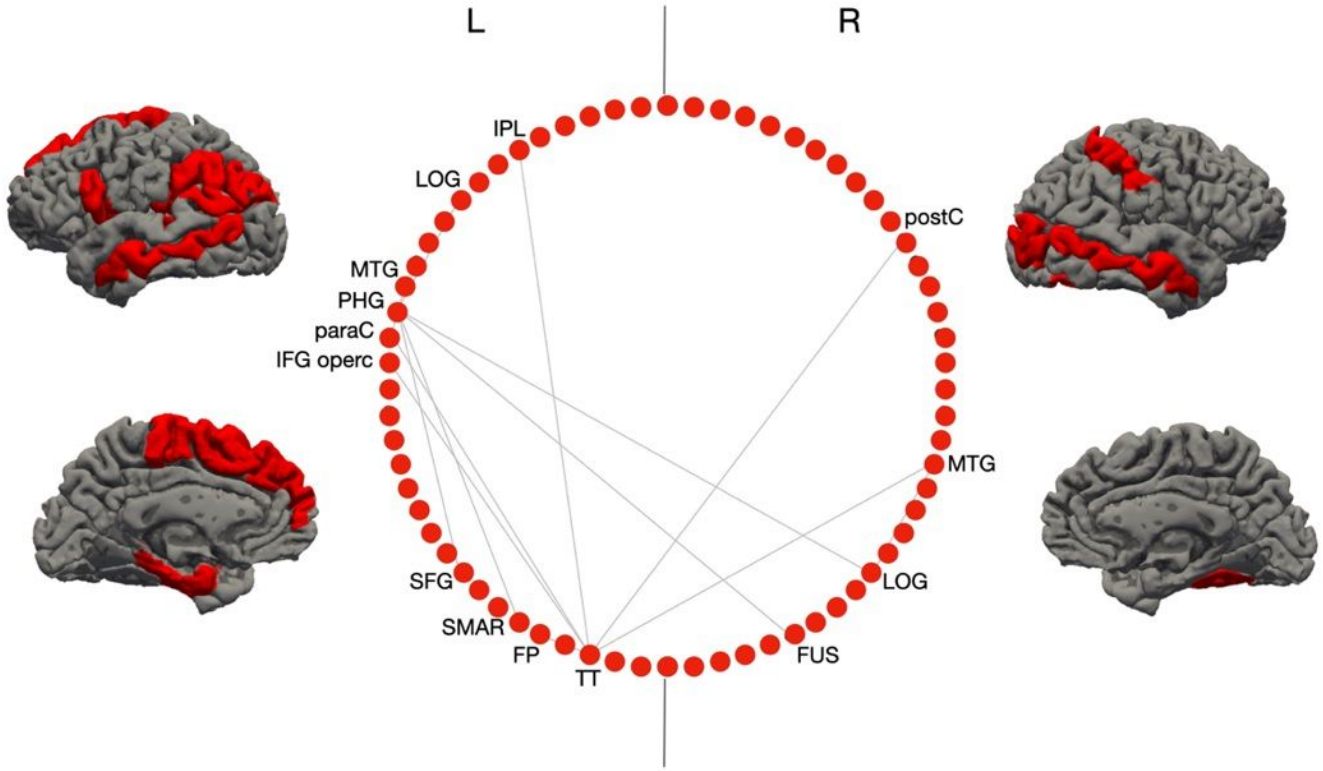

Figure 4

Regions with the most significant difference in inter-regional correlations of cortical thickness between groups: the inter-regional correlations for these regions were significantly greater for VH patients. Shown in the circular plot, only the inter-regional correlations with a difference greater than 0.3 in the r2 (for details and z scores on all differences, see S8). Legend: IPL = inferior parietal lobule; LOG = lat. Occipital gyrus; MTG = middle temporal gyrus; PHG = parahippocampal gyrus; paraC = paracentral gyrus; IFG opercularis. = inferior frontal gyrus; SFG = superior frontal gyrus; SMAR = supramarginal gyrus; FP = frontoparietal thickness; TT =temporal transverse; FUS = fusiform gyrus; postC = postcentral gyrus. The two vertical lines separate L and R hemisphere regions (left on left).

a) Cortical thickness - hubs:

Group	Hub Region
PD no VH	**L Superior frontal gy.**
	R Superior frontal gy.
	L Supramarginal gy.
	R Supramarginal gy.
	L Inf. Parietal lobule
	R Inf. Parietal lobule
	L Sup. Parietal lobule
	R Sup. Parietal lobule
	R Cuneus
	R Lat. Occipital gy.
PD VH	**L Superior frontal gy.**
	R r Middle Frontal gy.
	L r Middle Frontal gy.
	L Sup. Temporal gy.
	R Inf. Parietal Lobe

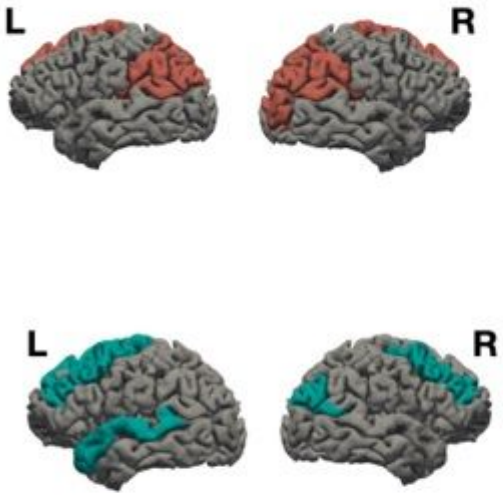

b) Communities

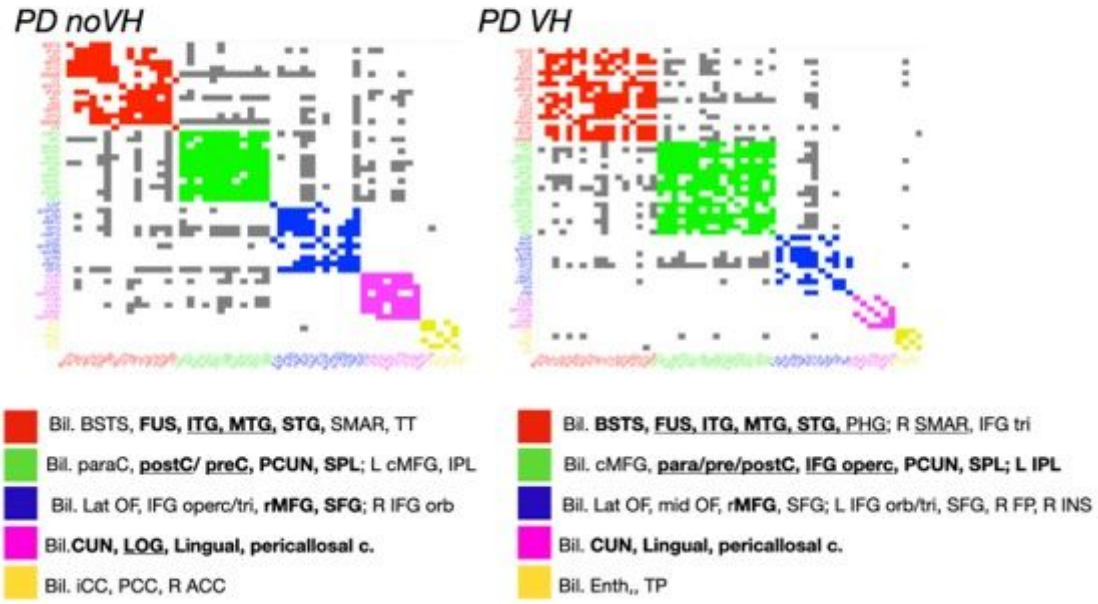

Figure 5

Hubs and communities: cortical thickness. a) Hubs identified based on efficiency, betweenness centrality and degree. Regions in bold are common hubs for both VH and noVH. b) Communities identified for each group. Legend: red = 1st community, green =2nd, blue= 3rd, pink = 4th, yellow = 5th. Only the first five communities are represented as they are the most informative ones. In bold the regions identified for that same community also in the surface area analysis. The regions underlined are the same regions presented in the figure with the regions with the greatest difference in inter-regional covariance. Legend: BSTS = banks superior temporal; IPL = inferior parietal lobule; SPL = superior parietal lobule; LOG = lat. Occipital gyrus; MTG = middle temporal gyrus; STG = superior temporal gyrus; cMFG = caudal middle

frontal gyrus; PHG = parahippocampal gyrus; paraC = paracentral gyrus; preC = precentral gyrus; postC = postcentral gyrus; IFG = inferior frontal gyrus; SFG = superior frontal gyrus; SMAR = supramarginal gyrus; FP = frontoparietal thickness; TT =temporal transverse; FUS = fusiform gyrus; CUN= cuneus.

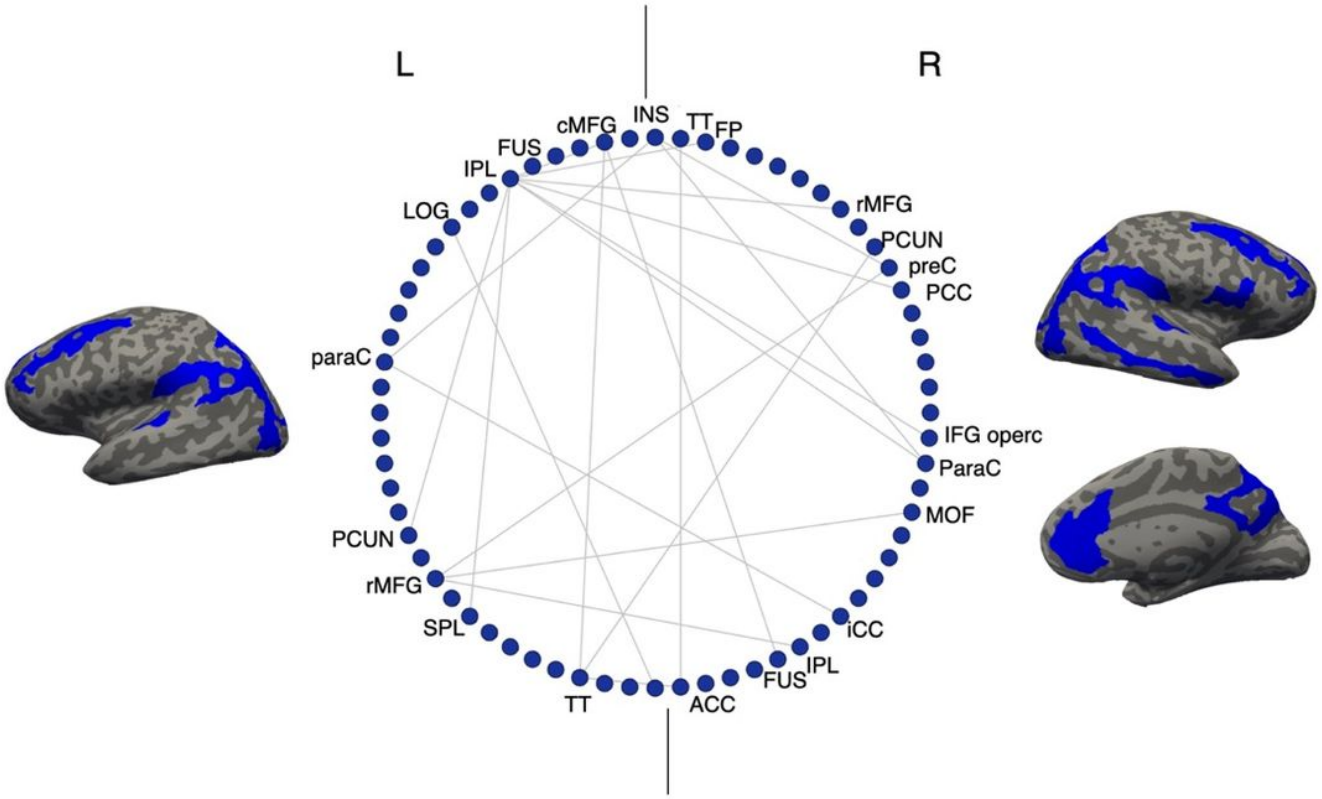

Figure 6

Regions with the most significant difference in inter-regional correlations of surface area between the groups: these correlations were significantly greater for PD-VH. Only the inter-regional correlations with a difference greater than 0.3 in the r2 are shown (for details see S8). Legend: IPL = inferior parietal lobule; SPL = superior parietal lobule; LOG = lat. Occipital gyrus; MTG = middle temporal gyrus; STG = superior temporal gyrus; cMFG = caudal middle frontal gyrus; PHG = parahippocampal gyrus; paraC = paracentral gyrus; preC = precentral gyrus; IFG = inferior frontal gyrus; SFG = superior frontal gyrus; SMAR = supramarginal gyrus; FP = frontoparietal thickness; TT = temporal transverse; FUS = fusiform gyrus; CUN= cuneus; PCUN = precuneus; MOF = middle orbitofrontal gyrus. The two vertical lines separate L and R hemisphere regions (left on left)

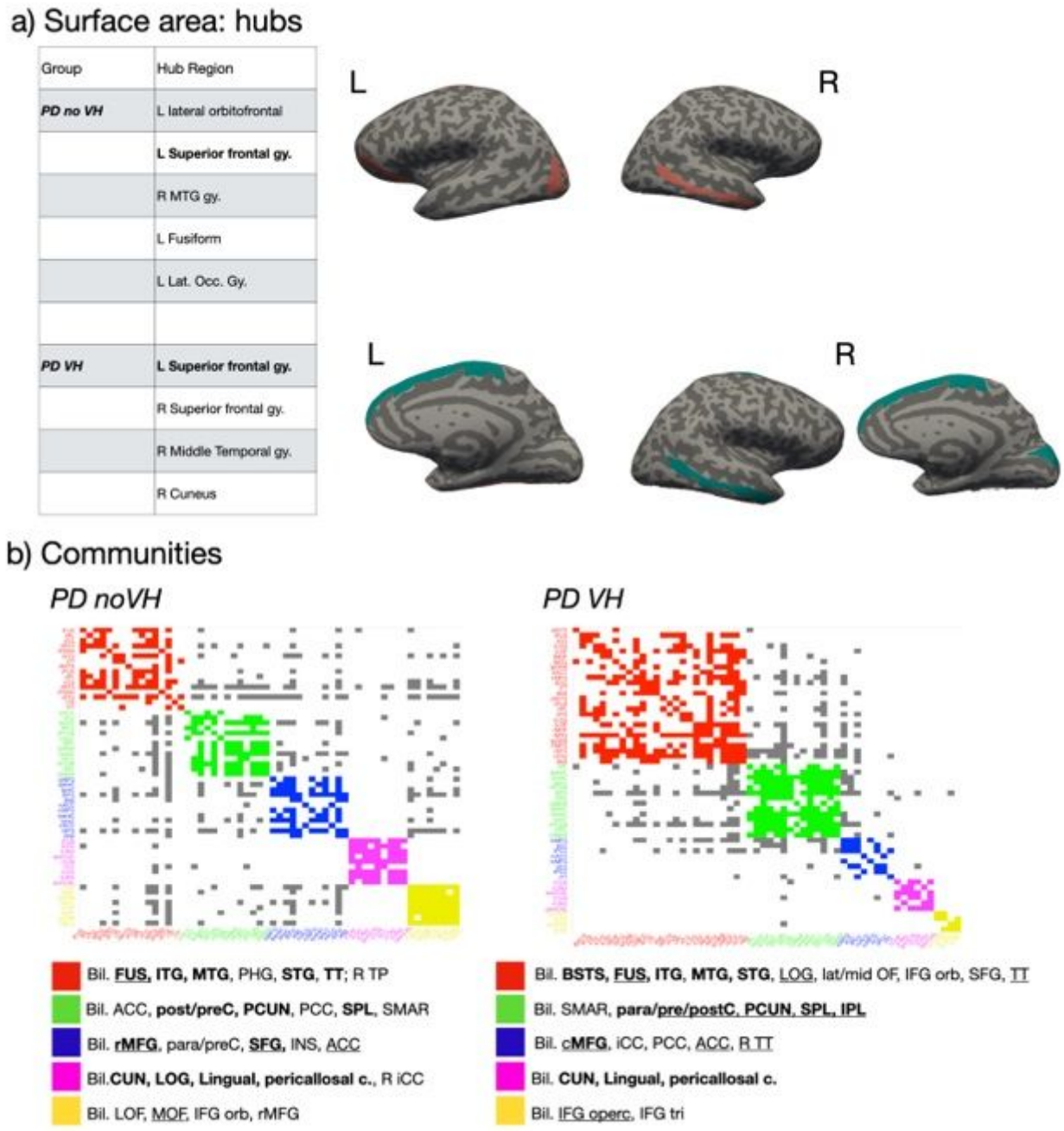

Figure 7

Hubs and communities: surface area. a) SA hubs identified based on efficiency, betweenness centrality and degree. Regions in bold are common hubs for both VH and noVH patients. b) Communities identified for each group. Legend: red = 1st community, green = 2nd, blue= 3rd, pink = 4th, yellow = 5th. In bold the regions identified for that same community also in the SA analysis. The regions underlined are the same regions presented in the figure with the regions with the greatest difference in inter-regional covariance. Legend: BSTS = banks superior temporal; IPL = inferior parietal lobule; SPL = superior parietal lobule; LOG = lat. Occipital gyrus; MTG = middle temporal gyrus; STG = superior temporal gyrus; ITG = inferior temporal gyrus; cMFG = caudal middle frontal gyrus; PHG = parahippocampal gyrus; paraC = paracentral

gyrus; preC = precentral gyrus; postC = postcentral gyrus; IFG = inferior frontal gyrus; SFG = superior frontal gyrus; SMAR = supramarginal gyrus; FP = frontoparietal thickness; TT = temporal transverse; FUS = fusiform gyrus; CUN= cuneus

Supplementary Files

This is a list of supplementary files associated with this preprint. Click to download.

- NCOMMS2107350.pdf
- MVignandoSupplementalInformation.docx